

Performance of a passive acoustic linear array in a tidal channel

Matthew Auvinen, David Barclay

Abstract

Baseline ambient sound level assessment is important in quantifying noise contributions from tidal energy infrastructure. Static acoustic sensing in high-flow conditions is complicated by pseudo-sound, or flow noise, generated by pressure fluctuations due to turbulent flow on the surface of a hydrophone. Signal processing methods are used to identify and suppress flow noise at low frequencies (< 500 Hz) in data collected on a four element horizontal hydrophone array in the Minas Passage, a tidal channel in the Bay of Fundy, in October 2016. Spectral slope analysis is used to identify the spectral critical frequency, where the flow noise and ambient noise contributions to the recorded signal are equal. Spatial coherence analysis is to identify the coherence critical frequency, where the first instance of flow noise occurs. The array's performance in the Minas passage is quantified by an empirical relationship between flow speed and the spectral critical frequencies of the coherent output from the liner array. Coherent averaging (broadside beamforming) is demonstrated as an effective flow noise suppression technique, improving low-frequency passive acoustic monitoring in a high energy tidal channel.

Index Terms

Flow noise, ambient noise, acoustical array, tidal channel, and passive acoustic monitoring.

I. INTRODUCTION

TIDAL power utilities are currently leasing seafloor space within the Minas Passage in the Bay of Fundy with aspirations of converting the energy of the region's tidal currents into electricity, a trend that has been supported by favorable projections of the Passage's tidal energy capacity [1]. As these companies seek sector development, it is important that they maintain sustainable industry practices.

Dr. David Barclay is an assistant professor in the Department of Oceanography, Dalhousie University. Matthew Auvinen holds a B.Sc. (Hons) from the Department of Oceanography, Dalhousie University, Halifax, NS (email: matthewauvinen@gmail.com; dbarclay@dal.ca).

Manuscript received June 30, 2017; revised MONTTH XX, 201X. This work was supported by the Natural Sciences and Engineering Research Council of Canada, GeoSpectrum Technologies, and Black Rock Tidal Power.

23 This includes the consideration of industry knowledge gaps, many of which are a consequence of the
24 sector's immaturity [2]. The uncertainty surrounding the ecological and environmental implications of
25 tidal turbine infrastructure is a particularly important knowledge gap and has qualified some opposition
26 to turbine projects.

27 Tidal turbines present two serious environmental threats: physical contact (or interaction) with marine
28 life [3] [4] and acoustic pollution.

29 Tidal turbines could become an important source of ambient noise in tidal channels through cavitation
30 and motor or mechanical noise [5]. Turbine anthropophony could affect animal navigation, communication,
31 predator-prey detections [6], and marine life cycles [7]. Moreover, turbine-generated sound could be
32 damaging to fish tissue [8]. If substantive, these effects will threaten near-field and far-field ecosystem
33 health, stressing the need for rigorous environmental impact assessments in the tidal power sector.

34 As a result, stakeholders, regulators, and tidal power companies are interested in establishing baseline
35 ambient noise measurements in the Minas Passage, against which turbine noise pollution will be measured.
36 However, the utility of ambient sensing is limited by pseudo-sound, or flow noise, generated on the surface
37 of a hydrophone in turbulent water. Indeed, the masking effects of flow noise can complicate source
38 identification and background noise assessment in high-flow settings, such as tidal channels.

39 Analogous to turbulent flowing air [9], flowing water in a high Reynolds number regime generates
40 pressure fluctuations on the surface of a hydrophone. These pressure fluctuations produce flow noise
41 which is irregular, uncorrelated, and random. Local pressure fluctuations on the surface of a hydrophone
42 represent near-field turbulence [10]. Free-drifting hydrophones moving with the mean water flow will
43 experience little signal contamination, as it is the relative flow of water over a hydrophone's surface that
44 leads to flow noise.

45 Turbulent flows occupy a wide range of frequencies and wavenumber domains, with broad spatial and
46 temporal variability. The advective nonlinearity of turbulent flows makes them unpredictable in space and
47 time, and contributes to their complex nature [11]. As such, it is difficult to reliably model flow noise
48 characteristics. Lombardi [6] identifies steep spectral slopes in measurements from a high-flow setting, an
49 artifact of small-scale turbulence averaged out across the surface of a submerged sensor. Bassett et al. [12]
50 further describes f^{-m} and identifies a spectral slope of $f^{-5/3}$ - not to be confused with the coincidental
51 wind-generated spectral slope, which occurs at higher frequencies [13] - below 20 Hz.

52 Flow noise presents a unique challenge for passive acoustic monitoring (PAM): a hydrophone in a

53 high-flow setting will record both propagating sound and pseudo-sound. This suggests that models should
54 distinguish between the two sound sources. Barclay and Buckingham [14] describe the exploitation of
55 uncorrelated flow noise to suppress pseudo-sound in deep ocean ambient noise measurements.

56 Successful suppression of flow noise could benefit PAM systems in the tidal energy sector. The objectives
57 of the present research are:

- 58 1) Use spectral analysis and spatial coherence to identify and characterize flow noise at low frequencies
59 (< 500 Hz).
- 60 2) Use coherent averaging (beamforming) to improve the performance of a linear hydrophone array
61 by suppressing flow noise and enhancing the measurement of ambient noise.

62 This paper is organized as follows. Section II discusses important field work details, including an
63 experiment description and instrumentation summary. Section III describes all relevant signal processing,
64 with emphasis on spectral analysis, spatial coherence, and beamforming. Section IV presents the signal
65 processing and data analysis results. Section V evaluates the results and identifies areas for future work.

66 Lastly, Section VI summarizes the findings of the study in a series of conclusions.

67 II. FIELD WORK

68 Field work was completed on October 27, 2016, near the Fundy Ocean Research Center for Energy
69 (FORCE) site in the Minas Passage of the Bay of Fundy. The deployment period spanned roughly four
70 hours, from 12:00 ADT to 16:00 ADT. This experimental window captured the transition from ebb tide
71 to slack tide.

72 Wind speed was measured intermittently throughout the deployment period using a hand-held wind
73 speed gauge and tidal data was generated using a WebTide model [15].

74 A. Experiment

75 A linear hydrophone array was streamed behind the *MV Nova Endeavour* (42' x 16'), which was
76 anchored to the seafloor in the Minas Passage. The array was positioned 15 meters below the sea surface
77 using a depressor. Four hydrophones were simultaneously sampled over a four hour period and processed
78 by an analog-to-digital converter (ADC) on board the *MV Nova Endeavour*. The signal cable, which
79 carried both the array and a drogue, was sheathed in a fairing to reduce strum generation and attached to
80 a tow cable (6GA galvanized wire) using cable ties.

81 A drifting hydrophone (Geospectrum Technologies GuardBuoy) was deployed using a small auxiliary
82 vessel launched from the *MV Nova Endeavour*. The GuardBuoy was suspended 2 meters below the surface
83 using a drifting surface float and isolation system made of spectra and compliant bungee. The system
84 isolated the recording hydrophone and instrument package from any surface action, such as the vertical
85 movement of waves, which would otherwise generate mechanical or flow noise.

86 A total of five transects were performed by driving the GuardBuoy upstream, deploying the drifter, then
87 floating downstream in a rigid-hulled inflatable boat (RHIB) alongside the GuardBuoy. The GuardBuoy
88 and RHIB followed a transect that passed over the array and then an additional 20 meters. These transects
89 were performed over the course of three hours, beginning at 13:00 ADT. The Guard Buoy signals are
90 assumed to be flow noise free and were used as benchmarks to assess the performance of the array. The
91 turbulent tidal channel is assumed to be well mixed with an isovelocity sound speed profile, minimizing
92 noise field variability over the depth difference between the two systems.

93 *B. Instrumentation*

94 The linear array was constructed by GeoSpectrum Technologies, and contains four sequentially spaced
95 hydrophones with a horizontal configuration. Each hydrophone pair is separated by a distance $d = 17\text{cm}$.
96 The array hydrophones were set to simultaneously sample at a rate of 96.038 kHz with an acoustic
97 bandwidth of 48.019 kHz. The four channels on the array continuously recorded 10 minute WAV files
98 over a 4 hour period. Power spectra were calibrated to dB re $1 \mu\text{Pa}$ according to frequency-dependent
99 sensitivities supplied by the manufacturer. The GuardBuoy sampled at a rate of 96 kHz with an acoustic
100 bandwidth of 48 kHz, and was equipped with a GPS to record transect geospatial information. The Guard
101 Buoy recorded WAV files in 30 minute segments. Corresponding power spectra were converted to dB re
102 $1 \mu\text{Pa}$ according to frequency-dependent sensitivities supplied by the manufacturer.

103 III. DATA ANALYSIS

104 Data analysis was performed in MATLAB in several stages. The analysis began with the calculation of
105 the power spectral density (PSD) from the raw WAV files, followed by spectral analysis, spatial coherence
106 analysis, and broadside beamforming.

¹⁰⁷ *A. General Signal Processing*

The output of a hydrophone is defined as

$$x_i(t) = \sigma_i(t) + n_i(t) \quad (1)$$

¹⁰⁸ where x_i is the recorded time series on each i th hydrophone, σ_i is the sound field's ambient components,
¹⁰⁹ and n_i is the locally generated flow noise. Importantly, n_i and σ_i are uncorrelated. Furthermore, the
¹¹⁰ inherent randomness of flow noise makes n_i incoherent with respect to n_j .

The power spectrum, or spectral density, is defined as

$$S_{ii}(\omega) = \frac{\langle X_i(\omega) \cdot X_i^*(\omega) \rangle}{T} \quad (2)$$

¹¹¹ where X_i is the Fourier transform of x_i , ω is angular frequency, $*$ denotes a complex conjugate, $\langle \rangle$
¹¹² indicates an ensemble average, and T is the observation interval. All Fourier transforms are windowed
¹¹³ by a Hann function. The Fourier transform is 2^{16} points long and contains 99 degrees of freedom.

Coherence is used to quantify the similarity between two signals and is defined as

$$\Gamma_{ij}(\omega) = \frac{S_{ij}(\omega)}{(S_{ii}(\omega) \cdot S_{jj}(\omega))^{\frac{1}{2}}}. \quad (3)$$

¹¹⁴ *B. Power Spectrum Probability Density*

¹¹⁵ Spectral probability density (SPD) is an analytical technique used to depict the variability of the power
¹¹⁶ spectrum over a period that is much longer than the minimum time required for a stationary measurement
¹¹⁷ of power to be made [16]. This form of analysis facilitates the identification of unique events within a
¹¹⁸ series of spectra.

The power spectrum probability density (PSPD) is defined as

$$\text{PSPD}(f) = H(S_{ii}(f), h) \quad (4)$$

¹¹⁹ where $\text{PSPD}(f)$ is the power spectrum probability density at frequency f , and $H(S(f), h)$ is the histogram
¹²⁰ of the power spectrum S_{ii} at frequency f with a histogram bin width of h dB re 1 μPa . By combining
¹²¹ PSPD results across frequencies, we generate a PSPD matrix

$$\begin{bmatrix} \text{PSPD}(f_1) & \text{PSPD}(f_2) & \text{PSPD}(f_3) & \dots & \text{PSPD}(f_a) \end{bmatrix} \quad (5)$$

122 where $\text{PSPD}(f_a)$ is the PSPD at the a th frequency.

123 *C. Spectral Critical Frequency*

124 Lombardi [6] and Bassett et al. [12] suggest that there are three distinct spectral slope regions in the
 125 low-to-mid-frequency range: Kolmogorov's $f^{-5/3}$ spectral slope; steepened flow noise spectral slopes of
 126 f^{-m} [12]; and an ambient noise region that is determined by near-field and far-field ambient sound sources.

The local spectral slope is defined as

$$f^{-M} = \frac{S_{ii}(2\pi f_a) - S_{ii}(2\pi f_b)}{\log(f_a \cdot f_b^{-1})} \quad (6)$$

127 where $S_{ii}(2\pi f_a)$ is the spectral density on the i th sensor at frequency f_a and $S_{ii}(2\pi f_b)$ is the spectral
 128 density on the i th sensor at frequency f_b . (6) describes the spectral slope in dB/decade.

The transition from the flow noise region of f^{-m} to the ambient noise region is marked by the frequency knee, where the spectral slope begins to shallow. That is, the exit from the flow noise region is marked by a deviation below the slope f^{-m} . Here, the spectral critical frequency, f_c , is defined as the first frequency at which

$$|f^{-M}| < |f^{-m}| \quad (7)$$

129 is true. Importantly, both slopes in (7) are in dB/decade.

130 *D. Coherence Critical Frequency*

131 Spatial coherence is calculated for each channel combination using (3), providing an assessment of
 132 signal similarity between elements. Propagating ambient noise is highly correlated across the array.
 133 Additionally, propagating noise at wavelengths sufficiently large relative to element spacing produces
 134 very high coherence at low frequencies by effectively co-locating sensors. Conversely, flow noise is a
 135 source of incoherence, as pseudo-sound is uncorrelated across the linear array (when turbulent scales are
 136 lesser than hydrophone separation). Therefore, in the band $f < 500$ Hz, flow noise is marked by low
 137 coherence while ambient noise is marked by high coherence. The transit of this coherence boundary, from
 138 flow noise (incoherent) to ambient noise (coherent) provides a metric for describing the extent of flow
 139 noise across the array.

The spatial coherence critical frequency, f'_c , is defined as the frequency at which a minimum coherence threshold is crossed. To establish this coherence threshold, we assume an isotropic ambient noise field such that the horizontal coherence is given by Buckingham [17]

$$G_{ij} = \frac{\sin(\omega'_{ij})}{\omega'_{ij}} \quad (8)$$

where

$$\omega'_{ij} = \frac{2\pi d_{ij} f}{c}. \quad (9)$$

Here, d_{ij} is the separation distance between the i th and j th hydrophone and c is the local sound speed. Formally, f'_c is the first frequency at which

$$|\Gamma_{ij}(\omega')| \geq 0.9 \cdot G_{ij} \quad (10)$$

is true. We can be confident that any coherence within 10% of (8) is real and significant while any drop below the threshold given by the right hand side of (10) is caused by incoherent noise. This automated critical frequency detector corresponds to coherence thresholds between 0.7 - 0.9 depending on the hydrophone separation distance.

144 E. Linear Regression

145 A linear regression between critical frequencies, f_c and f'_c , and flow speed, u , is used to identify and
 146 characterize the prevalence of flow noise and ambient noise in measurements. Importantly, no data points
 147 are excluded from this regression.

148 F. Beamforming

We use a broadside beamformer to coherently average the channels across the array. Locally generated flow noise and the ambient sound field are inseparable, however we can describe their relative prevalence with the theoretical signal-noise ratio (SNR) where we are defining ambient sound as the signal, and flow noise as the noise. By taking the Fourier transform of (1) and substituting into (2), we find

$$S_{ii} = \frac{\langle (\zeta_i + N_i) \cdot (\zeta_i^* + N_i^*) \rangle}{T} \quad (11)$$

where ς_i and N_i are the Fourier transforms of σ_i and n_i , respectively. For clarity, the frequency dependency has been omitted. Since ς_i and N_i are uncorrelated, we can expand (11) to arrive at

$$S_{ii} = \frac{\langle \varsigma_i \varsigma_i^* \rangle + \langle N_i N_i^* \rangle}{T}. \quad (12)$$

Given (12), the SNR for a single hydrophone (SNR_H) is defined as

$$\text{SNR}_H = \frac{\langle \varsigma_i \varsigma_i^* \rangle}{\langle N_i N_i^* \rangle} \quad (13)$$

where $\text{SNR}_H = 1$ at the critical frequency, f_c . Now consider an array of hydrophones indexed by i , where the ambient sound field component of the signal on each phone is

$$\sigma_{i+1}(t) = \sigma_1(t - \tau_i) \quad (i > 1) \quad (14)$$

where

$$\tau_i = \frac{i \cdot d \cos \theta}{c} \quad (15)$$

is the acoustic travel time in seconds for plane wave noise arriving on the sensors at the angle θ . Here, d is the nearest neighbour element separation. Taking the Fourier transform of (14) gives

$$\varsigma_i(\omega) = \varsigma_1(\omega) e^{-i\omega\tau_i}. \quad (16)$$

The coherent sum of the signals across the array is defined as

$$x_T(t) = \sum_{i=1}^l x_i(t) \quad (17)$$

where $x_i(t)$ is the signal recorded on the i th element of a linear array l elements long. Since no time delay has been applied to $x_i(t)$, $x_T(t)$ is the equivalent to beamforming broadside to the array. Since the source of interest is ambient noise, the sound field is assumed to be axially symmetric. Thus the horizontal array orientation and beam direction are unimportant, provided an appropriate array gain compensation is applied. The Fourier transform of (17) is

$$X_T(\omega) = \sum_{i=1}^l X_i(\omega). \quad (18)$$

The array power spectral density can be estimated using (18) by

$$A = \frac{\langle X_T(\omega) \cdot X_T^*(\omega) \rangle}{T}. \quad (19)$$

Given an array with both ambient noise and flow noise components, (18) can be expanded to

$$X_T = [\varsigma_1 + N_1 + \varsigma_2 + N_2 + \dots + \varsigma_l + N_l] \quad (20)$$

which describes the total output of all sensors on an array with l elements. Substituting (16) into (20) gives

$$X_T = \varsigma_1 + N_1 + \sum_{i=1}^l (\varsigma_i e^{-i\omega\tau_i} + N_{i+1}). \quad (21)$$

Using the Fourier transform of the coherently summed outputs across the array, the power spectral density can be computed by substituting (21) into (19) yielding

$$A = \frac{\langle \varsigma_1 \varsigma_1^* \left[l + \sum_{i=1}^{l-1} \frac{1}{2} (l-i) \cos(\omega\tau_i) \right] + N \cdot N^* \rangle}{T} \quad (22)$$

where

$$N = \sum_i^l N_i \quad (23)$$

is the coherently summed flow noise. This term can be simplified by assuming the power of the flow noise measured on each individual hydrophone is equal across the array,

$$\langle N_i N_i^* \rangle = \langle N_j N_j^* \rangle \quad (24)$$

and uncorrelated between the sensors,

$$\langle N_i N_j^* \rangle = \delta_{ij} \cdot N_1 N_1^* \quad (25)$$

$$\delta_{ij} = \begin{cases} 0 & \text{if } i \neq j \\ 1 & \text{if } i = j. \end{cases}$$

Then the total power received by the array becomes

$$A = \frac{\langle \varsigma_1 \varsigma_1^* \rangle \left[l + \sum_{i=1}^{l-1} \frac{1}{2} (l-i) \cos(\omega \tau_i) \right] + l \langle N_1 N_1^* \rangle}{T}. \quad (26)$$

Furthermore, if K is defined as

$$K = l + \sum_{i=1}^{l-1} \frac{1}{2} (l-i) \cos(\omega \tau_i) \quad (27)$$

then (26) becomes

$$A = \frac{K \langle \varsigma_1 \varsigma_1^* \rangle + l \langle N_1 N_1^* \rangle}{T} \quad (28)$$

where (28) describes the array spectral density. Here, SNR_A describes the relative strength of the ambient noise and flow noise components of the array output, such that

$$SNR_A = \frac{K \langle \varsigma_1 \varsigma_1^* \rangle}{l \langle N_1 N_1^* \rangle}. \quad (29)$$

Comparing (29) to the result derived for a single hydrophone, given by (13), we see that the beamformed array improves the signal-to-noise ratio by a factor of $\frac{K}{l}$. Furthermore, (29) suggests that array performance improves with an increasing number of hydrophones, l . For an array with 4 elements, at broadside, $\frac{K}{l} = \frac{7}{4}$.

154 G. Array Gain

The broadside beamforming analysis applied to the linear array generates artificial spectral density gain. As a result, an array gain formula is applied to the beamformed results to correct the inflated values. The array gain formula presented here is adapted from Cox [18], such that

$$AG = 20 \log l. \quad (30)$$

155 The array gain correction is performed by subtracting the result of (30) from the calculated array power
156 spectral density.

157 *H. Algorithm Assessment*

158 (18) and (19) are used to consolidate all channel signals into one coherent array output. The coherent
 159 array spectral critical frequencies are compared to the spectral critical frequencies of a fixed single
 160 hydrophone to critically evaluate the performance of the beamformed array. GuardBuoy, fixed single
 161 hydrophone, and coherent array signals are compared to further assess the coherent array's performance.

162 **IV. RESULTS**

163 *A. Spectral Density*

164 Signal levels (Fig. 1) are relatively high in fast flowing water and low in slow flowing water. The
 165 mid-to-high-frequency band is less affected by flow noise and is quiet relative to lower frequencies (<
 166 10 Hz). Evidently, flow noise is prevalent below 100 Hz.

167 The wind speed varied between 3.2 and 6.2 m/s with a mean of 5.0 m/s. The hydrophone power
 168 spectrum contains multiple episodes of mid-frequency noise. These signals are attributed to ship noise
 169 generated by the small vessel used in the GuardBuoy drifter tests. Additionally, the abrupt shift in spectral
 170 density at 90 minutes is due to equipment reconfigurations.

171 *B. Power Spectrum Probability Density*

172 The PSPD facilitates the broad-scale assessment of a hydrophone's spectral density over entire deploy-
 173 ment periods. The PSPD for channel 0 is shown in Fig. 2.

174 The PSPD follows a spectral slope of $f^{-5/3}$ below 10 Hz, behaviour analogous to Kolmogorov's
 175 turbulence theory. This spectral slope marks a region of flow noise within the signal. A steepened spectral
 176 slope of f^{-m} , where $m > \frac{5}{3}$, persists between 10 and 100 Hz, a result of small-scale turbulence when
 177 turbulence wavelength \ll sensor size. This small-scale turbulence is averaged out over the surface of
 178 the hydrophone sensor, dampening the measured signals. The PSPD results show that ambient noise is
 179 dominant above 300 Hz, where signal levels are markedly low. Early in the deployment (around 10
 180 minutes) electronic noise in the system raised the noise floor to 90 dB μPa . While this was quickly
 181 remedied on site, an electronic system noise floor persisted at about 60 dB re μPa .

182 Single power spectra are superimposed on the PSPD and suggest that measurements in slow current
 183 conditions contain a greater extent of ambient noise relative to those in fast current conditions.

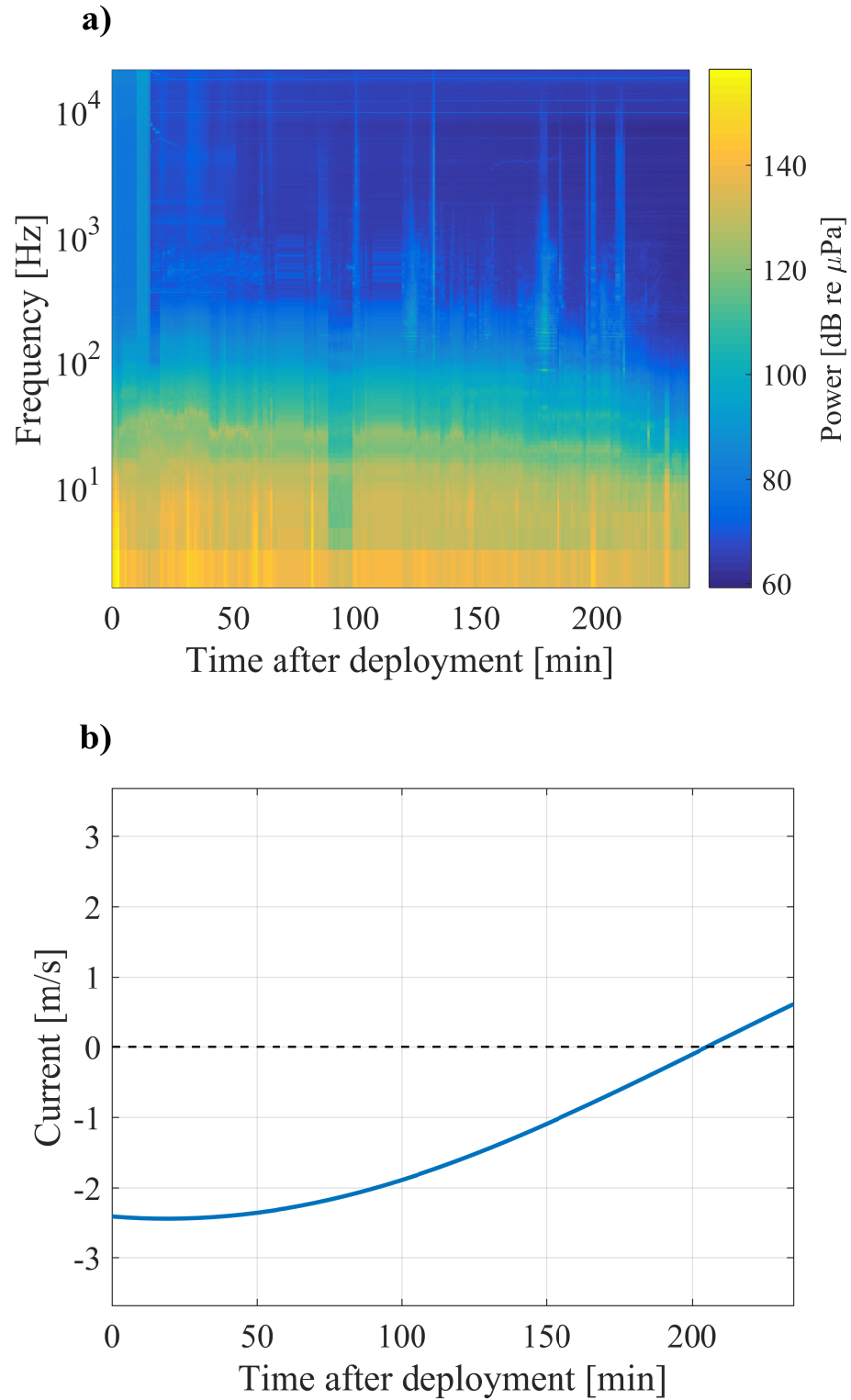


Fig. 1. Power spectrum for channel 0 on the array (a). The spectrum is plotted over the deployment period across a range of low-to-mid frequencies. The spectrum begins at maximum ebb tide and ends at slack tide, as shown by the current time series (b). Power decreases with flow speed over the deployment period.

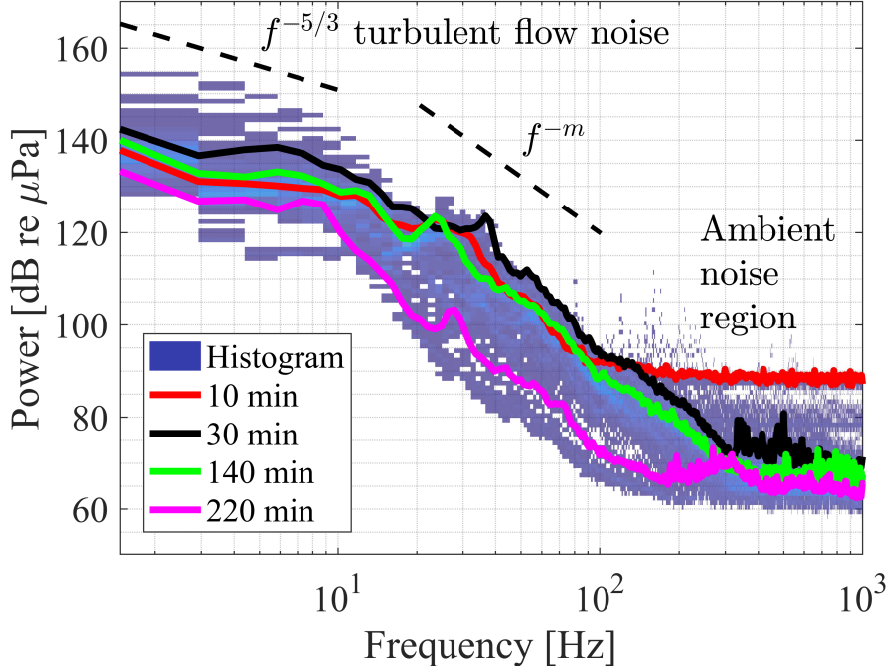


Fig. 2. Channel 0 power spectrum probability density over the entire deployment period. Turbulent flow noise is prevalent < 10 Hz (where wavelengths \gg sensor size), with a spectral slope of $f^{-5/3}$, while turbulence interacting with the hydrophone's finite size (in the 10 Hz to 100 Hz band) yields a spectral slope of f^{-m} . The ambient sound field dominates at < 300 Hz. Time indicates the elapsed time after deployment for each superimposed fixed hydrophone signal spectra.

184 C. Spectral Critical Frequency

185 (6) was used to iteratively calculate the spectral slope between 10 and 100 Hz. The linear relationship
 186 between spectral slope, f^{-m} , and current, u , (Fig. 3) indicates that signals recorded in decreasing flow
 187 are increasingly damped (steepened slope). The inverse relationship between current speed and spectral
 188 slope suggests that signals are less damped in fast flowing water, a result of larger turbulence scales.
 189 The spectral slopes observed between 10 and 100 Hz range from -25 to -60 dB/decade. The correlation
 190 coefficient, R , suggests that there is a meaningful correlation between spectral slope and current.

191 The spectral critical frequency was iteratively calculated over the experimental period using (7). These
 192 critical frequencies were regressed against current, as shown in Fig. 4. There is a positive correlation
 193 between spectral critical frequency and current speed, where fast flow coincides with high spectral critical
 194 frequencies. As such, the spectral critical frequency is used to track the transition from the flow noise
 195 region to the ambient noise region.

196 Importantly, the intercepts have not been forced to zero. This is because it is unrealistic to expect that
 197 we can completely eliminate flow noise, or low-frequency noise generated by the mechanical systems that

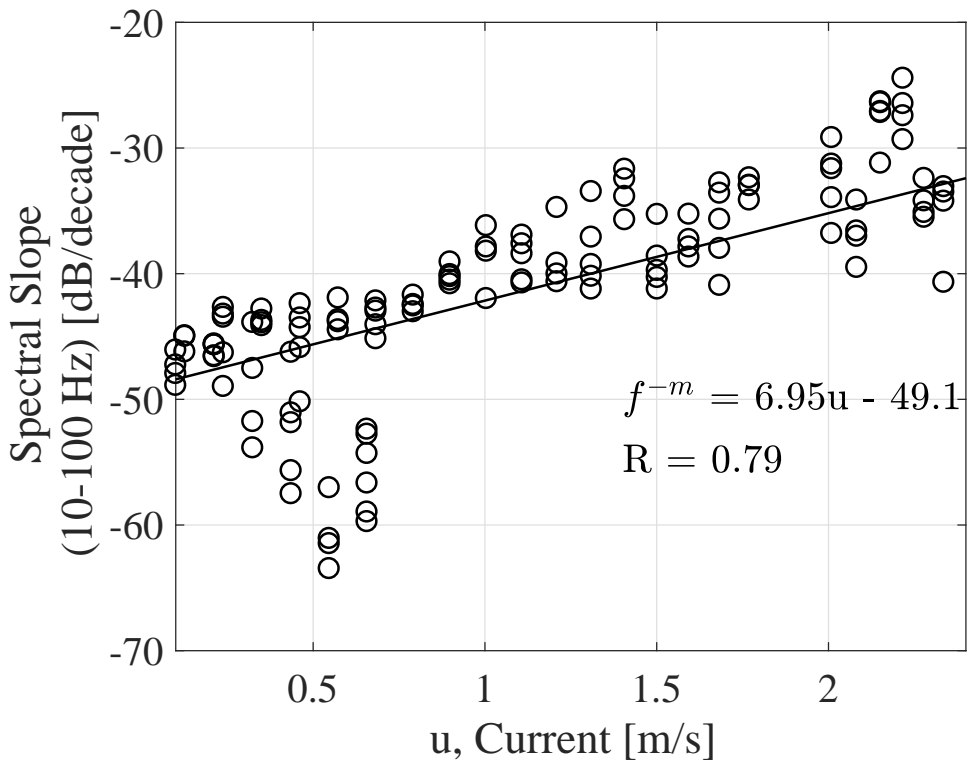


Fig. 3. Relationship between spectral slope, f^{-m} , and current, u , between 10 and 100 Hz for channel 0. Spectral slope magnitude increases with decreasing flow. Spectral slopes are steeper than Knudsen's -17 dB./decade. Correlation coefficients, R , are reported.

198 comprise the tow body. If this were a moored system with no surface expression, that assumption might
199 be valid, but is not considered here.

200 *D. Spatial Coherence*

201 Spatial coherence is calculated for different hydrophone combinations across the linear array using
202 (3). The spatial coherence results are presented in magnitude coherence for the entire deployment period
203 (Fig. 5). If the wavelength of propagating sound is sufficiently long (frequency sufficiently low) the
204 sensors would become relatively co-located and the coherence would tend to unity. However, the results
205 suggest that the low frequency data is overwhelmingly incoherent, since the locally generated flow noise
206 is incoherent from one hydrophone to the next.

207 Flow noise is uncorrelated and propagating ambient noise is highly correlated at low frequencies. As
208 a result, low coherence and high coherence are a sign of flow noise and ambient noise, respectively.
209 Therefore, the spatial coherence results are partitioned into two distinct regions: a flow noise region
210 and an ambient noise region. Visual assessment suggests that flow noise is consistently present at low
211 frequencies and can be prominent at higher frequencies (above 600 Hz). The ambient noise region is

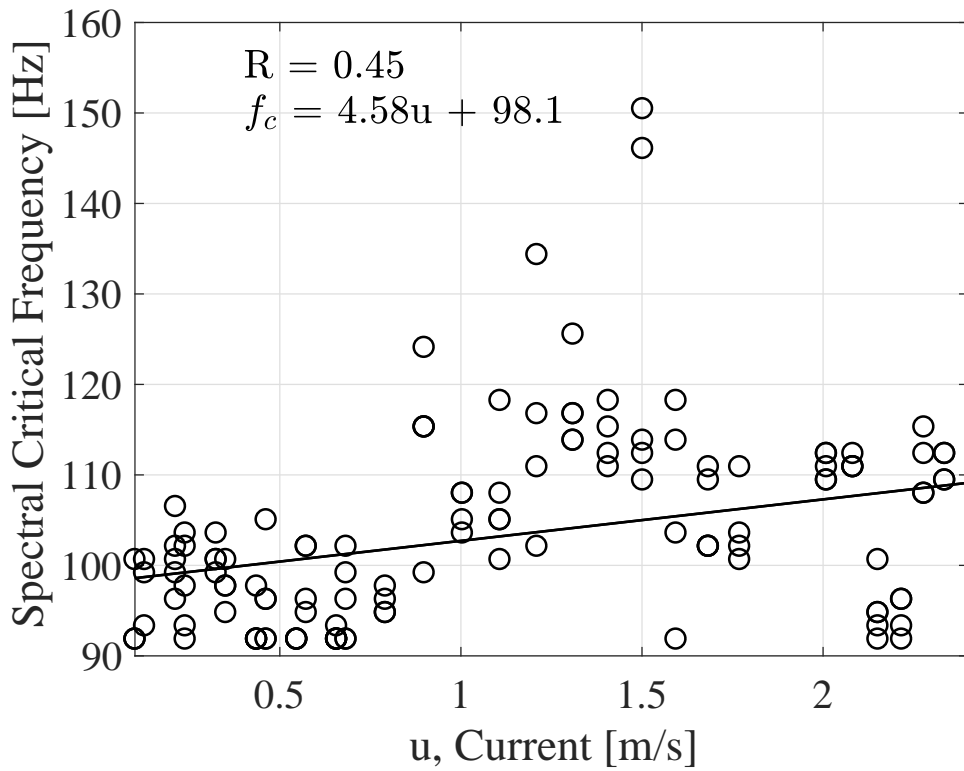


Fig. 4. Relationship between spectral critical frequency, f_c , and current, u , for channel 0. Spectral critical frequency reveals where flow noise is no longer dominant. Correlation coefficients, R , are reported.

212 present between 200 and 600 Hz and contains the same vessel noise identified in Fig. 2.

213 *E. Coherence Critical Frequency*

214 The coherence critical frequency is the frequency at which the boundary between the ambient noise and
 215 flow noise regions occurs. The coherence critical frequency was iteratively calculated for each combination
 216 of channels, and is used to quantify the relative prevalence of flow noise and ambient noise within
 217 a measurement (Fig. 6). The coherence critical frequency is a more sensitive method of flow noise
 218 measurement than the spectral critical frequency, as spatial coherence is an indicator of flow noise cessation
 219 rather than relative noise contributions. The coherence critical frequency increases with increasing flow
 220 speed, a relationship similar to that of the spectral critical frequency.

221 It is important to note that the coherence is impacted by any temporary deterministic noises present in
 222 the sound field, such as the auxiliary RHIB, mechanical array noise, or noise generated aboard the *MV*
 223 *Nova Endeavour*. In such instances, the automated coherence critical frequency detector fails, and yields
 224 an outlier.

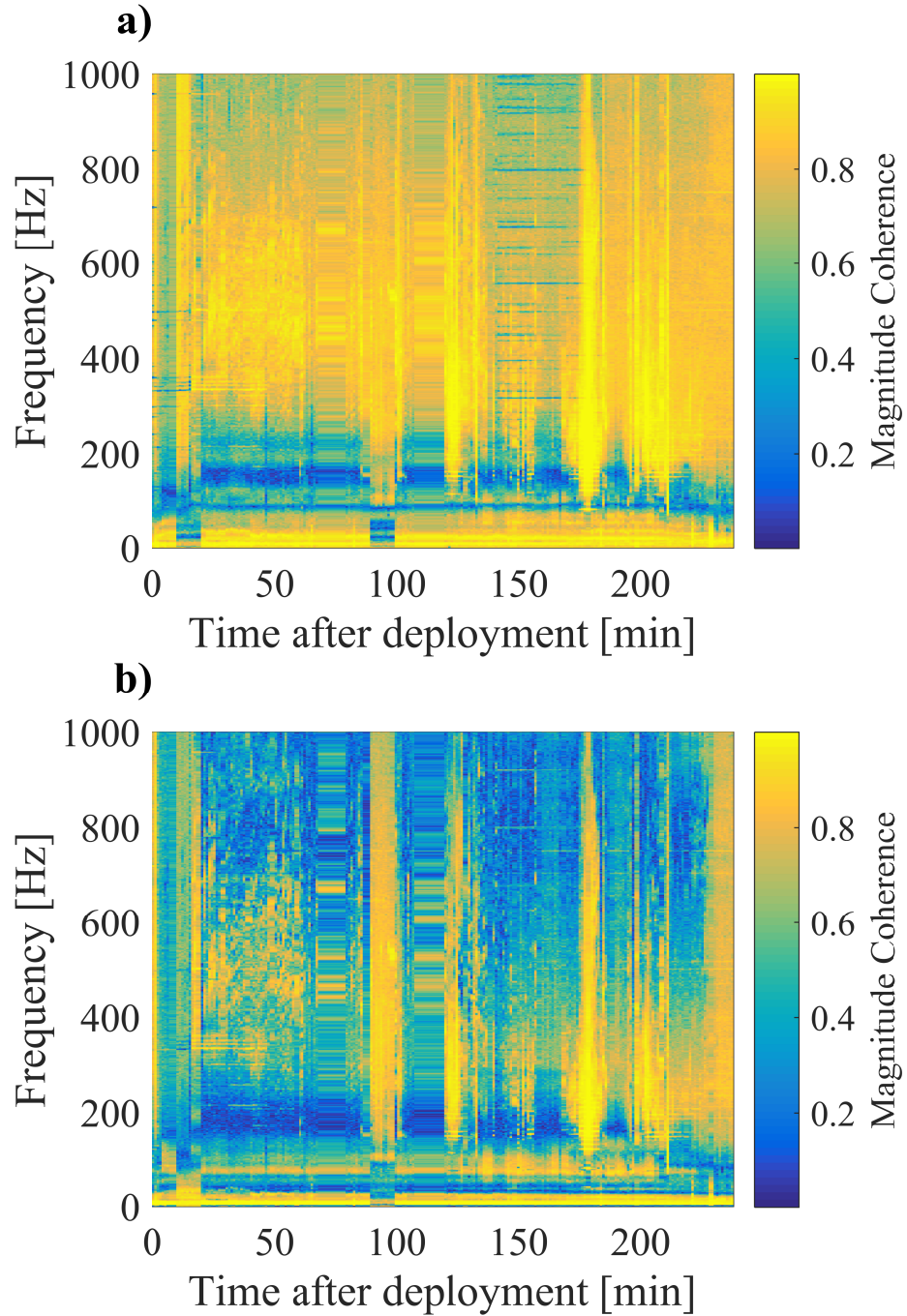


Fig. 5. Spatial coherence over the experimental period. Magnitude coherence is expected to tend to unity as the hydrophones become relatively co-located. However, uncorrelated flow noise on each phone breaks that relationship. Incoherent flow noise regions increase with current speed. Channel 0 - 1 (a) and 0 - 3 (b) are shown as examples. Results hold to all other channel combinations.

225 There is a good deal of noise in Fig. 6, as no outliers nor oddities were discarded. The retention of
 226 outliers is done to maintain the integrity of the linear regression and the correlation present.

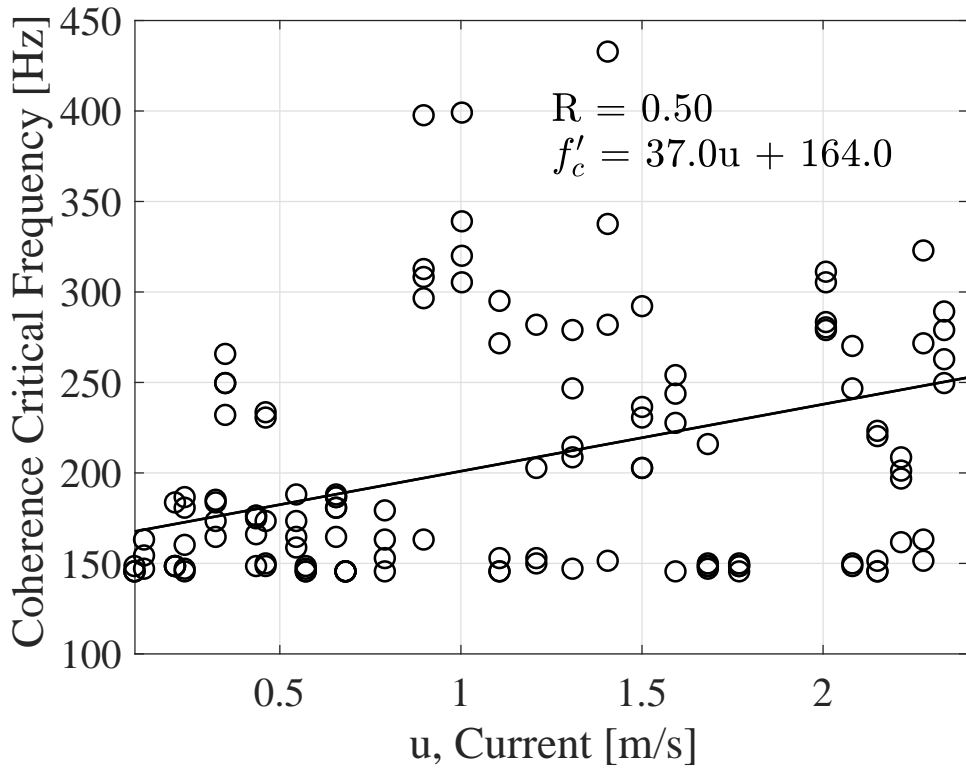


Fig. 6. Relationship between coherence critical frequency, f'_c , and current, u , for channels 0 - 1. Coherence critical frequency is used to detect the critical frequency in a more precise way than the spectral approach.

227 F. Beamforming

228 The spectral critical frequency of the coherent array output is compared to the fixed single hydrophone
 229 spectral and coherence critical frequencies in Fig. 7. The standard deviations of the spectral slope and
 230 spatial coherence critical frequency regressions were extracted from the averaged fits, while the standard
 231 deviation of the coherent array critical frequency regression was calculated from the data during the
 232 regression.

233 The coherence critical frequencies are relatively high, while spectral critical frequencies (both fixed
 234 single hydrophone and coherent array) are relatively low. This is attributed to the more sensitive nature
 235 of the coherence-based method. Above coherence critical frequencies we can be confident that there
 236 is no contamination of the ambient noise field by flow noise. Conversely, the fixed single hydrophone
 237 and coherent array thresholds show where flow noise is dominant. The coherence and spectral critical
 238 frequencies serve as the respective upper and lower bounds of different noise regimes. Importantly, the
 239 coherent array contains significantly lower critical frequencies than the fixed single hydrophone, indicating
 240 that the broadside beamforming approach lessens the extent of flow noise within the measurements.

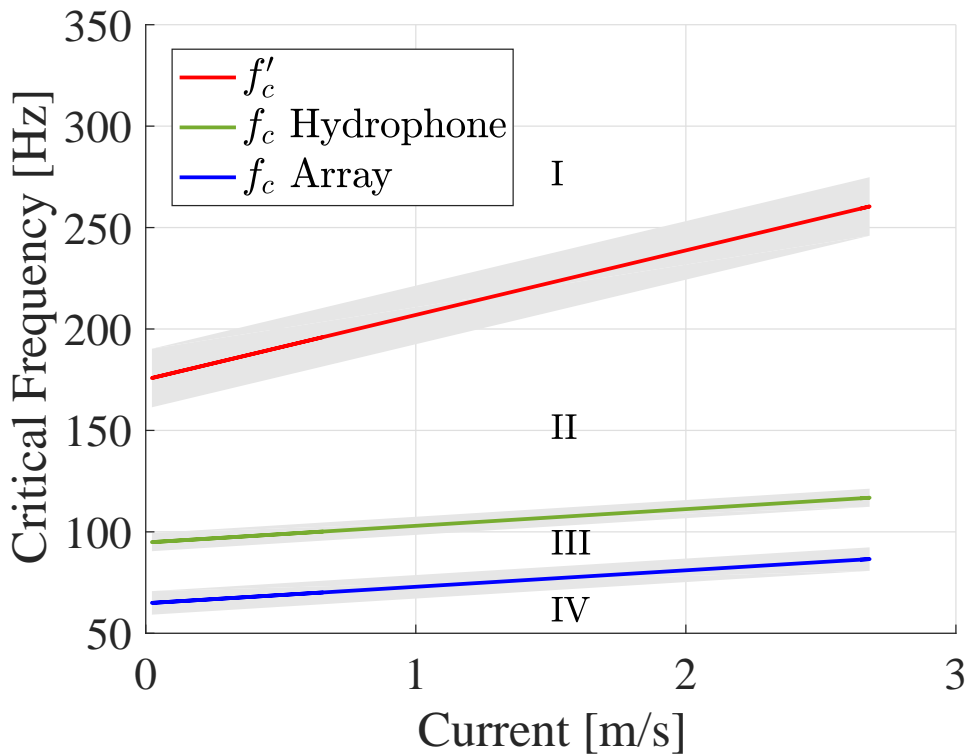


Fig. 7. Comparison of hydrophone spectral critical frequency, coherence critical frequency, and array spectral critical frequency distributions. Coherence and spectral critical frequencies reveal regions of flow noise, ambient noise, and a mixture of both. Uncertainties are one standard deviation (shaded). I is an ambient noise region, II is a region of ambient noise and flow noise, III is a region of flow noise measured on a fixed single hydrophone, and IV is a region of flow noise measured on the coherent array.

241 Fig. 8 compares GuardBuoy, fixed single hydrophone, and horizontal coherent array power spectra at
 242 1.5 hours into the experiment. We select a time where the drifter and array were in close proximity to
 243 establish a meaningful comparison.

244 The GuardBuoy spectrum behaves differently from the rest, exhibiting lower levels at frequencies
 245 below 100 Hz. A pronounced excursion in spectral slope is present at 10 Hz in the GuardBuoy spectrum,
 246 suggesting non-negligible flow noise is affecting the drifter's low-frequency measurements. This is typical
 247 of all moored or free drifting passive acoustic systems that have a surface expression or subsurface float.
 248 The fixed single hydrophone shows clear symptoms of flow noise at low frequencies.

249 The spectra reveal that the coherent array spectra transitions to the ambient noise region at lower
 250 frequencies than the fixed single hydrophone. Furthermore, the coherent array signals are quieter than
 251 the fixed single hydrophone signals at all low frequencies, demonstrating the effective suppression of
 252 flow noise. There is reasonable agreement between the GuardBuoy and coherent array above the critical
 253 frequency, with some difference above 700 Hz. This disparity is attributed to the lack of co-location
 254 between the array and the GuardBuoy, as they are vertically and horizontally displaced relative to each

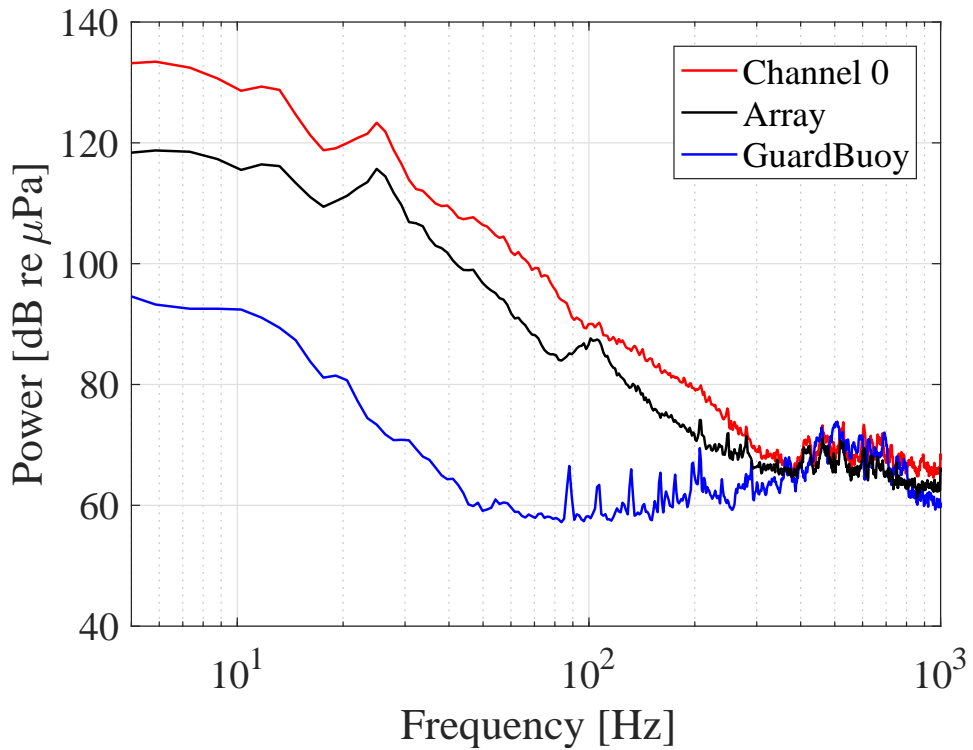


Fig. 8. Comparison of channel 0 (fixed single hydrophone), coherent array, and GuardBuoy signal power spectra at 1.5 hr into the deployment.

255 other.

256

V. DISCUSSION

257 A. Spectral Critical Frequency

258 Results show that critical frequency and flow speed are positively related, giving the intuitive result
 259 that flow noise is prevalent in fast current conditions. The spectral critical frequency presents a method
 260 of identifying flow noise prevalence within a signal.

261 The spectral critical frequency provides two important insights. Firstly, frequencies above the spectral
 262 critical frequency will contain a mixture of ambient noise and flow noise, since the threshold marks the
 263 reduction in flow noise, and not its absence. Secondly, frequencies below the critical frequency will be
 264 dominated by flow noise, since measurements in these frequencies contain spectral slopes that align with
 265 turbulence theory. These insights are important, as they provide useful context for future signal level and
 266 sound-source evaluations in tidal channel measurements.

267 *B. Spatial Coherence*

268 Spatial coherence results for different sensor combinations show that there are two distinct coherence
269 regions across the array: an incoherent flow noise region and a coherent ambient noise region. The
270 prevalence of these regions is quantified with the coherence critical frequency. Iterative calculations of the
271 coherence critical frequency were regressed against current speed. There is a positive relationship between
272 coherence critical frequency and current speed. The coherence critical frequency marks the frequency above
273 which flow noise is absent.

274 The spectral critical frequency provides a lower boundary, below which only flow noise exists, and
275 the coherence critical frequency provides an upper boundary, above which only ambient noise exists.
276 Frequencies between these bounds contain a mixture of flow noise and ambient noise. This explains why
277 the coherence critical frequencies are noticeably higher than those of the spectral method. The application
278 of spectral and coherence critical frequencies provides insight on the relative extent of both ambient noise
279 and flow noise within a signal.

280 *C. Beamforming*

281 By effectively treating the array as one sensor or hydrophone, signal processing can address the pseudo-
282 sound within low frequency data. Coherent averaging suppresses flow noise and enhances the detection of
283 propagating ambient noise. The coherent averaging employs a broadside approach with no steering angle
284 (19).

285 The results of the beamformed array are shown in Fig. 7. Evidently, the coherent array contains lower
286 levels and lower critical frequencies than the fixed single hydrophone (Fig. 8). This implies that the
287 coherent array is less affected by flow noise, and contains a greater extent of ambient noise.

288 Further research would help support the findings of this project. This includes longer testing periods,
289 experimentation in different flow conditions, and tests in different bathymetric settings. Elimination of the
290 mechanical noise floor would strengthen the present research. It would also be advantageous to conduct
291 tests with arrays of different length and a varied number of elements.

292 VI. CONCLUSION

293 Flow noise appears in two regions: as $f^{-5/3}$ noise when wavelength \gg sensor size, and as f^{-m} , where
294 the sensor's finite dimension reduces the flow noise. f^{-m} is related to the flow speed over the array. A

295 spectrum's deviation from f^{-m} slope indicates where flow noise is no longer dominant. Spatial coherence
296 can be used to identify when the effect of flow noise is negligible.

297 Coherent processing (beamforming) suppresses flow noise and yields a lower spectral critical frequency
298 at all flow speeds than that of a fixed single hydrophone. An increased number of hydrophones and
299 array length could improve array performance, allowing passive acoustic monitoring at arbitrarily low
300 frequencies.

301

REFERENCES

- 302 [1] R. Karsten, A. Swan, and J. Culina, "Assessment of arrays of in-stream tidal turbines in the Bay of Fundy," *Phil. Trans. R. Soc. A*,
303 vol. 371, no. 1985, p. 20120189, 2013.
- 304 [2] R. Inger, M. J. Attrill, S. Bearhop, A. C. Broderick, W. James Grecian, D. J. Hodgson, C. Mills, E. Sheehan, S. C. Votier, M. J. Witt
305 *et al.*, "Marine renewable energy: potential benefits to biodiversity? An urgent call for research," *Journal of Applied Ecology*, vol. 46,
306 no. 6, pp. 1145–1153, 2009.
- 307 [3] M. J. Dadswell, "Occurrence and migration of fishes in Minas Passage and their potential for tidal turbine interaction," 2010.
- 308 [4] A. Redden and M. Stokesbury, "Acoustic tracking of fish movements in the Minas Passage and FORCE demonstration area: Pre-turbine
309 baseline studies (2011-2013)."
- 310 [5] D. Wang, M. Atlar, and R. Sampson, "An experimental investigation on cavitation, noise, and slipstream characteristics of ocean stream
311 turbines," *Proceedings of the Institution of Mechanical Engineers, Part A: Journal of Power and Energy*, vol. 221, no. 2, pp. 219–231,
312 2007.
- 313 [6] A. Lombardi, "Soundscape characterization in Grand Passage, Nova Scotia, a planned in-stream tidal energy site," 2016.
- 314 [7] M. K. Pine, A. G. Jeffs, and C. A. Radford, "Turbine sound may influence the metamorphosis behaviour of estuarine crab megalopae,"
315 *PLoS One*, vol. 7, no. 12, p. e51790, 2012.
- 316 [8] M. Halvorsen, T. Carlson, and A. Copping, "Effects of tidal turbine noise on fish," *PNNL Report-20787 for US Dept of Energy*, WA,
317 DC: by Pacific Northwest National Laboratory, Sequim, WA, pp. 1–41, 2011.
- 318 [9] M. Lighthill, "The Bakerian lecture, 1961. Sound generated aerodynamically," in *Proceedings of the Royal Society of London A:
319 Mathematical, Physical and Engineering Sciences*, vol. 267, no. 1329. The Royal Society, 1962, pp. 147–182.
- 320 [10] M. Strasberg, "Nonacoustic noise interference in measurements of infrasonic ambient noise," *The Journal of the Acoustical Society of
321 America*, vol. 66, no. 5, pp. 1487–1493, 1979.
- 322 [11] M. Van Dyke, *An album of fluid motion*. Parabolic Press Stanford, 1982, vol. 176.
- 323 [12] C. Bassett, J. Thomson, P. H. Dahl, and B. Polagye, "Flow-noise and turbulence in two tidal channels," *The Journal of the Acoustical
324 Society of America*, vol. 135, no. 4, pp. 1764–1774, 2014.
- 325 [13] V. O. Knudsen, R. Alford, and J. Emling, "Underwater ambient noise," *J. Mar. Res.*, vol. 7, pp. 410–429, 1948.
- 326 [14] D. R. Barclay and M. J. Buckingham, "Depth dependence of wind-driven, broadband ambient noise in the Philippine Sea," *The Journal
327 of the Acoustical Society of America*, vol. 133, no. 1, pp. 62–71, 2013.
- 328 [15] F. Dupont, C. G. Hannah, and D. Greenberg, "Modelling the sea level of the upper Bay of Fundy," *Atmosphere-Ocean*, vol. 43, no. 1,
329 pp. 33–47, 2005.
- 330 [16] N. D. Merchant, T. R. Barton, P. M. Thompson, E. Pirotta, D. T. Dakin, and J. Dorocicz, "Spectral probability density as a tool for
331 ambient noise analysis," *The Journal of the Acoustical Society of America*, vol. 133, no. 4, pp. EL262–EL267, 2013.

- 332 [17] M. J. Buckingham, "On the two-point cross-correlation function of anisotropic, spatially homogeneous ambient noise in the ocean and
333 its relationship to the Greens function," *The Journal of the Acoustical Society of America*, vol. 129, no. 6, pp. 3562–3576, 2011.
334 [18] H. Cox, "Line array performance when the signal coherence is spatially dependent," *The Journal of the Acoustical Society of America*,
335 vol. 54, no. 6, pp. 1743–1746, 1973.

336 **Matthew Auvinen** Biography text here.

PLACE
PHOTO
HERE

337

338 **David Barclay** Biography text here.

PLACE
PHOTO
HERE

339